

CO signatures in subtropical convective clouds and anvils during CRYSTAL-FACE: An analysis of convective transport and entrainment using observations and a cloud-resolving model

Jimena P. Lopez,¹ Ann M. Fridlind,² Hans-Jürg Jost,¹ Max Loewenstein,²
 Andrew S. Ackerman,² Teresa L. Campos,³ Elliot M. Weinstock,⁴ David S. Sayres,⁴
 Jessica B. Smith,⁴ Jasna V. Pittman,⁴ A. Gannet Hallar,² Linnea M. Avallone,⁵
 Sean M. Davis,⁵ and Robert L. Herman⁶

Received 20 April 2005; revised 4 November 2005; accepted 10 January 2006; published 6 May 2006.

[1] Convective systems are an important mechanism in the transport of boundary layer air into the upper troposphere. The Cirrus Regional Study of Tropical Anvils and Cirrus Layers–Florida Area Cirrus Experiment (CRYSTAL-FACE) campaign, in July 2002, was developed as a comprehensive atmospheric mission to improve knowledge of subtropical cirrus systems and their roles in regional and global climate. In situ measurements of carbon monoxide (CO), water vapor (H₂O_v), and total water (H₂O_t) aboard NASA’s WB-57F aircraft and CO aboard the U.S. Navy’s Twin Otter aircraft were obtained to study the role of convective transport. Three flights sampled convective outflow on 11, 16 and 29 July found varying degrees of CO enhancement relative to the free troposphere. A cloud-resolving model used the in situ observations and meteorological fields to study these three systems. Several methods of filtering the observations were devised here using ice water content, relative humidity with respect to ice, and particle number concentration as a means to statistically sample the model results to represent the flight tracks. A weighted histogram based on ice water content observations was then used to sample the simulations for the three flights. In addition, because the observations occurred in the convective outflow cirrus and not in the storm cores, the model was used to estimate the maximum CO within the convective systems. In general, anvil-level air parcels contained an estimated 20–40% boundary layer air in the analyzed storms.

Citation: Lopez, J. P., et al. (2006), CO signatures in subtropical convective clouds and anvils during CRYSTAL-FACE: An analysis of convective transport and entrainment using observations and a cloud-resolving model, *J. Geophys. Res.*, *111*, D09305, doi:10.1029/2005JD006104.

1. Introduction

[2] It has been widely recognized that convective systems play an important role in the transport of boundary layer pollutants into the upper troposphere and lower stratosphere [Chatfield and Crutzen, 1984; Dickerson et al., 1987; Pickering et al., 1990, 1996; Prather and Jacobs, 1997; Thompson et al., 1994]. For example, Pickering et al. [2001] found that the South Pacific Convergence Zone (SPCZ) is an important climatological feature that can

establish ozone (O₃) and other trace gas distributions in the southwestern tropical Pacific in the middle to upper troposphere. This convective transport of atmospheric tracers to the upper troposphere generally depends upon the strength and the structure of the updrafts and downdrafts, as well as the chemical composition of the boundary layer and the free troposphere, which can vary in nature [Randriambelo et al., 2000; Scala et al., 1990].

[3] There have been a number of trace gas experiments in convective clouds conducted in past decades (see Table 1). For example, the Preliminary Regional Experiment for Stormscale Operational and Meteorology Program-Central Phase (PRESTORM) project investigated the role of summertime convection in the south central United States, in particular in Oklahoma [Luke et al., 1992]. This study provided the first direct observation of convective transport of largely undiluted boundary layer tracers to the upper troposphere in an anvil core [Dickerson et al., 1987]. In contrast, it also demonstrated that not all cases of convection lead to substantial upper tropospheric concentrations from polluted boundary layers [Pickering et al., 1988].

¹Bay Area Environmental Research Institute, Sonoma, California, USA.

²NASA Ames Research Center, Moffett Field, California, USA.

³National Center for Atmospheric Research, Boulder, Colorado, USA.

⁴Department of Earth and Planetary Sciences, Harvard University, Cambridge, Massachusetts, USA.

⁵Program in Atmospheric and Oceanic Sciences, University of Colorado, Boulder, Colorado, USA.

⁶Jet Propulsion Lab, Pasadena, California, USA.

Table 1. Convective Tracer Transport Studies in the Past Decades

Project	Location	Date	References
GATE	West Africa	September 1974	<i>Pickering et al.</i> [1998]
PRESTORM	central United States	June 1985	<i>Bernardet et al.</i> [2000], <i>Dickerson et al.</i> [1987], <i>Luke et al.</i> [1992], <i>Park et al.</i> [2004], <i>Pickering et al.</i> [1989, 1992], <i>Pickering et al.</i> [1988, 1990, 1995, 1998], <i>Thompson et al.</i> [1994]
ABLE IIA	Brazil	August 1985	<i>Garstang et al.</i> [1988], <i>Pickering et al.</i> [1992], <i>Pickering et al.</i> [1991], <i>Thompson et al.</i> [1997]
EMEX-STEP	Australia and New Guinea	February 1987	<i>Danielson</i> [1993], <i>Pickering et al.</i> [1993, 1998]
ABLE IIB	Brazil	April–May 1987	<i>Pickering et al.</i> [1992], <i>Pickering et al.</i> [1993, 1998], <i>Scala et al.</i> [1990], <i>Thompson et al.</i> [1997]
North Dakota Thunderstorm Project	North Dakota	June 1989	<i>Poulida et al.</i> [1996], <i>Stenchikov et al.</i> [1996]
ROSE	Alabama	June 1990	<i>Lin et al.</i> [1994]
CLEOPATRA	southern Germany	Summer 1992	<i>Hauf et al.</i> [1995]
TRACE-A	equatorial and tropical South Atlantic	September–October 1992	<i>Mari et al.</i> [2000], <i>Pickering et al.</i> [1996, 1998], <i>Smyth et al.</i> [1996], <i>Thompson et al.</i> [1997]
Case Study over British Isles	United Kingdom	October 1992	<i>Gimson</i> [1997]
TOGA-COARE	western Pacific	February 1993	<i>Pickering et al.</i> [1998]
CEPEX	central and equatorial Pacific	April 1993	<i>Wang and Crutzen</i> [1995], <i>Wang and Prinn</i> [1998]
ASHOE/MAESA	Fiji	October 1994	<i>Folkins et al.</i> [1997]
STERAO	northeastern Colorado	July 1996	<i>Barth et al.</i> [2001, 2004], <i>DeCaria et al.</i> [2000], <i>Decaria et al.</i> [2005], <i>Dye et al.</i> [2000], <i>Skamarock et al.</i> [2000]
PEM-Tropics A	South Pacific	September 1996	<i>Fenn et al.</i> [1999], <i>Wang et al.</i> [2000]
EULINOX	Germany	July 1998	<i>Fehr et al.</i> [2004]
PEM-Tropics B	South Pacific	March 1999	<i>Mari et al.</i> [2003], <i>Pickering et al.</i> [2001]
TRACE-P	Pacific Basin	March–April 2001	<i>Kiley et al.</i> [2003], <i>Liu et al.</i> [2003]
MINOS	Mediterranean	August 2001	<i>Fischer et al.</i> [2003]
CRYSTAL-FACE	Florida	July 2002	<i>Xueref et al.</i> [2004], this work

[4] There have also been many modeling analyses performed on convective systems. For instance, a deep convective storm observed on 3 April 1993, during the Central Equatorial Pacific Experiment (CEPEX) project was simulated using a two-dimensional cloud dynamics, microphysics and chemical model using O_3 as a passive boundary layer tracer [*Wang et al.*, 1995]. Wang et al. found that the O_3 redistribution caused by transport and mixing during the mature stage of the simulated storm was significant. Their initial conditions were constrained using an O_3 sounding and assuming horizontal homogeneity. They found, from the model, that convective storms, while producing upward transport of tropospheric air into the tropical stratosphere, also can produce downward transport from the stratosphere into the troposphere. Due to the differences in upward and downward directed transports, the net mixing effect of a thunderstorm can be different at each distinct altitude. Overall, it was determined that horizontal wind profiles must be carefully treated in two-dimensional and three-dimensional numerical simulations of convective transport of trace gases [*Wang and Prinn*, 1998] in order to accurately constrain entrainment.

[5] Similarly, during the Cloud Dynamics and Chemistry Field Experiment (CLEOPATRA), O_3 and water vapor (H_2O_v) measurements were made with the German Falcon aircraft in the cloudy outflow of a convective system over southern Germany in 1992 [*Hauf et al.*, 1995]. A three-dimensional, time-dependent, mesoscale model was then used to simulate the thunderstorm. They found an undiluted core of boundary layer air within the anvil cloud that extended vertically and horizontally over the entire length (120 km) of the storm with a large O_3 mixing ratio near the cloud edges. This core eventually eroded due to environ-

mental entrainment at the edges. This simulation suggests that boundary layer air can stay relatively undiluted during the convective transport process and thereby affect large areas downwind of a storm.

[6] During the Transport and Atmospheric Chemistry Near the Equator-Atlantic (TRACE-A) project [*Smyth et al.*, 1996], the convective pumping of biomass burning pollution to the upper troposphere was studied using a one-dimensional detraining/entraining plume model with carbon monoxide (CO) as a passive tracer of boundary layer pollution [*Mari et al.*, 2000]. The CO boundary layer mixing ratio was high (350 ppb) due to biomass burning influence leading to a postconvective upper troposphere CO-layer mixing ratio of over 200 ppb in both the model and the observations. They found that more than half of the CO entrained in the cloud was from the 7–15 km region of the free troposphere, while 40% was entrained below the cloud base. This finding is consistent with other studies that found significant entrainment from the midtroposphere [*Dickerson et al.*, 1987; *Scala et al.*, 1990; *Wang and Chang*, 1993; *Wang et al.*, 1995]. It was also found that deep convection in Brazil and southern Africa can transport ozone precursors to the upper troposphere [*Pickering et al.*, 1996; *Thompson et al.*, 1996].

[7] A companion project to TRACE-A, TRACE-P (Pacific), designed to characterize the chemical composition of Asian outflow and to describe its evolution over the Pacific Basin [*Jacob et al.*, 2003], included support from several three-dimensional chemical transport models (CTMs). These models were intercompared and evaluated for TRACE-P. The DC-8 flight on 27 March 2000 designed to study middle and high-level outflow over Southeast Asia and China. It was found that convection can reduce air mass

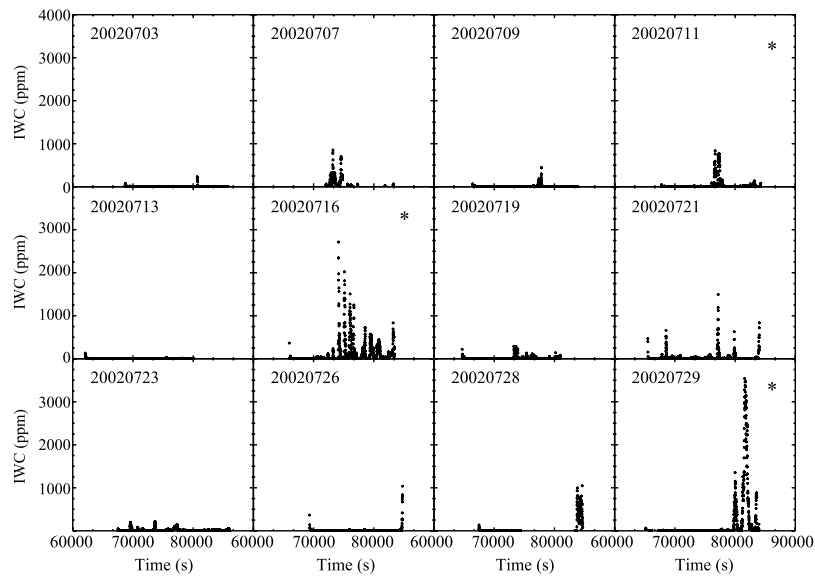


Figure 1. Overview of all CRYSTAL-FACE science flights shown as IWC time series. These data are used to determine the convection-influenced flights for this cloud resolving model tracer transport study. The asterisks in the right corner of the subplot indicate flights studied in this manuscript.

integrity because updrafts and downdrafts within the convective column will mix air masses of different history [Kiley *et al.*, 2003]. Thus one can be confident in a back trajectory reaching an individual convective system but can be less certain about any prior convective encounters.

[8] Convective systems occurring during the Stratospheric-Tropospheric Experiment: Radiation, Aerosols and Ozone (STERAO)-Deep Convection campaign during summer of 1996 in northeastern Colorado were studied extensively due to the high frequency of varied storms in the area. In a case study, it was found that the strong convective system on 10 July was effective in transporting boundary layer tracers, in particular CO, from the surface to the upper troposphere with relatively little entrainment of mid and upper tropospheric air into the storm core [Dye *et al.*, 2000]. This was simulated in a three-dimensional nonhydrostatic cloud model and with similar low out-of-cloud air entrainment and mixing occurring in the updrafts [Skamarock *et al.*, 2000]. In addition, this STERAO flight was used in an intercomparison of tracer transport in deep convection using a variety of convective scale models [Barth *et al.*, 2004]. Initial out-of-cloud conditions were provided to the models. In general, model-predicted CO mixing ratios agreed relatively well with observations, especially in the anvil core. The edges of convective systems, however, were not predicted as well. In addition, most models overpredicted the CO flux and air mass flux.

[9] Storms in a variety of locations have been studied in the past (Table 1). However, on the basis of trace gas observations, a large variability has been noted in the ability of the storms to transport boundary layer air to the upper troposphere. Many of the storm experiments were designed to examine transport, and the convective systems were therefore well characterized, but this is not the case for all studies. Overall, statistical methods of comparing the simulations with flight observations have relied on particle

number concentrations, meteorological conditions, tracer observations and temporal sampling, but have not been studied in detail. This paper is focused on CO as a convective transport tracer, with a low-altitude aircraft providing the boundary layer (0–5 km) measurements and a high-altitude aircraft providing the upper tropospheric (8–20 km) measurements. In addition, other observations, in particular ice water content, are used here to statistically compare model results with observations. We will focus on three convective case studies.

2. CRYSTAL-FACE

2.1. Project Goals

[10] The Cirrus Regional Study of Tropical Anvils (CRYSTAL) was developed as a comprehensive atmospheric mission to improve knowledge of tropical cirrus systems and their role in regional and global climate. The Florida Area Cirrus Experiment component of CRYSTAL (CRYSTAL-FACE) took place during July 2002 in Key West, Florida. Its objective was to study the production and evolution of convective systems and cirrus clouds in a subtropical region in preparation for a future tropical component of CRYSTAL [Jensen *et al.*, 2004]. Two of the participating aircraft (the U.S. Navy's Twin Otter and NASA's WB-57F) contained the in situ tracer measurements, with the majority of the tracers on the WB-57F aircraft. The in situ tracers measured on the WB-57F included CO, methane (CH₄), O₃, carbon dioxide (CO₂), H₂Ov, total water (H₂Ot), nitric oxide (NO) and total reactive nitrogen (NO_y), while the Twin Otter in situ measurements included only CO and H₂Ov measurements.

[11] The broad goal of detailed large-eddy simulations of CRYSTAL-FACE case studies [Fridlind *et al.*, 2004; Xueref *et al.*, 2004] has been to draw together myriad independent observations into a quantitatively integrated understanding of the coupled dynamical and microphysical processes

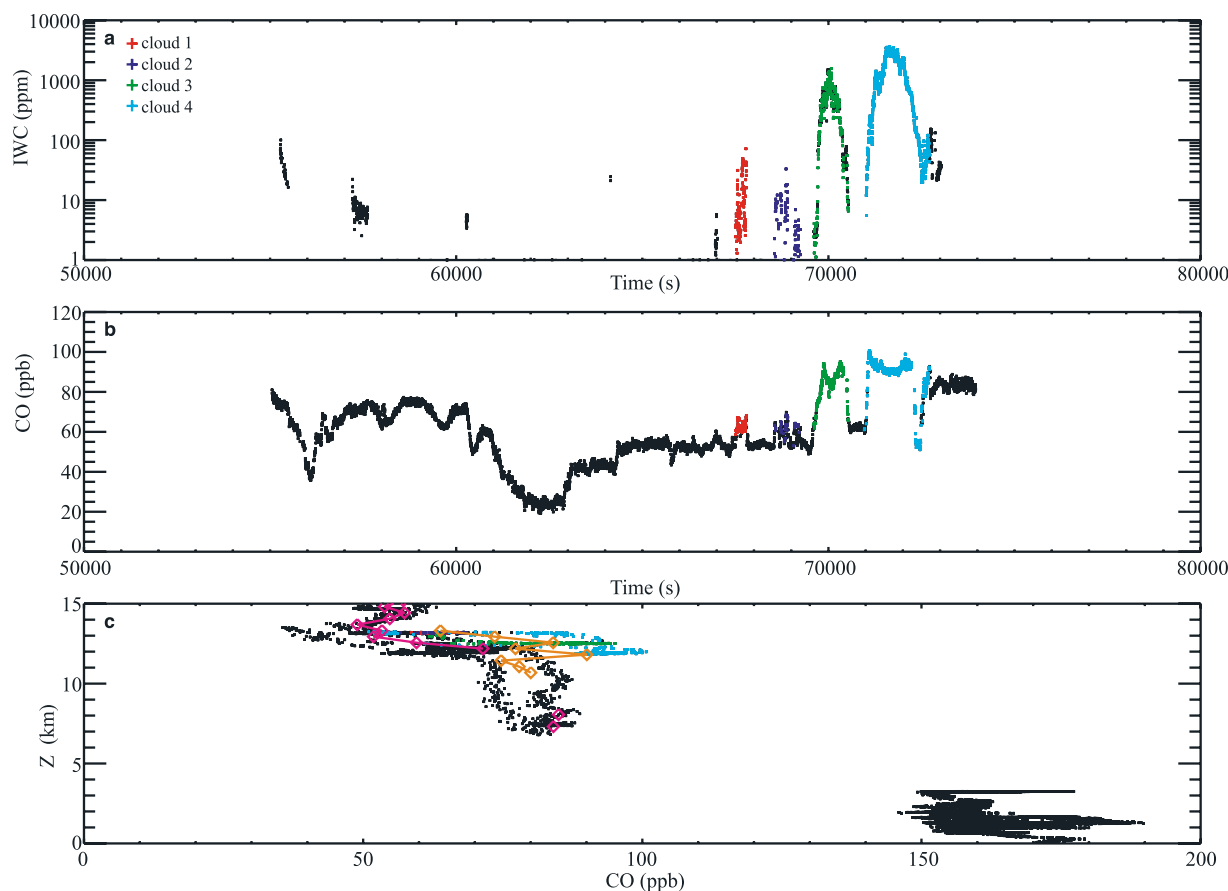


Figure 2. Demonstration of selecting in-cloud air parcels using the flight of 29 July as an example. The four significant flight passes through the convective outflow are each marked in a different color. The color scheme remains consistent through the three different plots: (a) IWC with respect to flight time, (b) CO with respect to flight time, and (c) altitude with respect to CO. Orange and violet diamonds in Figure 2c represent the altitude binned in-cloud and out-of-cloud, respectively. CO mixing ratios are as defined in the text.

during Florida deep convection. Here we focus on a set of passive tracer measurements made during the experiment. The narrower goal of this particular analysis is to use the measurements to quantitatively evaluate modeled tracer fields. Because storms are highly chaotic and our simulations are only statistical in representation, point-to-point comparisons cannot be made. Assuming that initial and boundary conditions are known, the primary problem encountered during evaluation of simulated four-dimensional tracer fields is therefore that of statistically sampling the modeled fields consistently with the sparse measurements, which were made in this case via aircraft. The approach we take here is to use other measurements made on the aircraft to statistically sample the model results in an effort to compare “apples with apples” (observed regions of cirrus outflow with regions of similar cloud density in the simulated anvil, for instance). We also make rough estimates of the uncertainty associated with incomplete measurement of initial and boundary conditions. Finally, we provide our best estimate of average error between model results and observations on each day obtained with our statistical sampling technique.

2.2. CRYSTAL-FACE Flight Descriptions

[12] During CRYSTAL-FACE, twelve science flights with multiple objectives were conducted on the WB-57F. Three of those twelve WB-57F flights presented themselves as suitable case studies for convective transport of tracers, which are long-lived, relative to the lifetime of a storm. These included the flights of 11, 16, and 29 July, all of which sampled the peripheries of strong convective systems, as demonstrated by the ice water content (IWC) plots shown in Figure 1 and by radar images of the cloud cover over Florida during those flights (<http://angler.larc.nasa.gov/crystal/>). The IWC was calculated both from the combination of the Harvard University Lyman-alpha H₂O_t and H₂O_v instruments [Weinstock *et al.*, 1994] and from the combination of JPL’s H₂O_v [Herman *et al.*, 2002] and University of Colorado’s H₂O_t [Haller *et al.*, 2004] instruments. The calculated IWC values were similar for the Harvard and JPL/CU instruments. For simplicity, Harvard’s IWC is the only data shown here. Many of the other flights that showed high IWC either were not tied to an obvious local convective system (e.g., 7 and 28 July) or were not well sampled during flight (e.g., 21 July).

[13] Deep convection over the Florida peninsula is strongly diurnal, developing in an environment of strong surface heating and moisture convergence. A typical day's convection over south Florida begins with the development of small cells, often in lines, in late morning and early afternoon near the coast, often in association with sea breeze fronts. Development moves inland during the midafternoon hours, with new cells breeding on the outflow boundary convergence of decaying cells. By late afternoon, it is not atypical that the field of convection is dominated by a few large cells or groups of cells, generating large but relatively short-lived anvils that span large fractions of the region. In the evening and nighttime hours, further convective development moves offshore. The storm in each of the case studies formed in different areas over or near the Florida peninsula, and this is reflected in the results. The three convective cases were sampled at different stages of storm development. The storms were not sampled in or above the convective cores, but instead were sampled in the anvil blowoff and at the edges of the convective system.

2.3. Observational Data and Instrumentation

[14] The CO measurements on the WB-57F were collected with NASA-Ames Research Center's tunable diode laser spectrometer, Argus, a small, lightweight, dual channel instrument capable of measuring atmospheric mixing ratios of CO and CH₄ at a data rate of 0.5 Hertz [Loewenstein *et al.*, 2002]. The accuracy of Argus, to one-sigma, is approximately 3%, with a precision value of near 2 ppb for CO. The lower troposphere CO on the Twin Otter was measured using a resonance fluorescence (RF) technique in the fourth positive band of CO [Gerbig *et al.*, 1999]. The RF and Argus instruments intercompare well (within measurement errors of 3–5%) within the atmospheric dynamic range sampled during CRYSTAL-FACE (not shown).

[15] In order to analyze the time series data in terms of convective transport to the upper troposphere, the air influenced by convection was identified as air with an IWC greater than 1 ppm. Both IWC measurements (Harvard University and CU) agreed on the presence of ice at this threshold. Cloud-free regions were identified where IWC was less than 1 ppm. In addition, only cloud-free regions upwind of the convective storm of interest were used in order to minimize memory effects due to the storms passing through an area. All data, regardless of instrument, were binned using interpolation between 10-s time intervals to put data on the same time stamp.

[16] An example of how an individual cloud event is defined in a convective system is shown in Figure 2, using the flight on 29 July as a sample case. The WB-57F aircraft encountered a convective storm near the end of the flight. Figure 2a shows a time series plot, binned at 10-s intervals, for IWC. Whenever IWC was greater than 1 ppm and persisted for at least 30 s, it was marked with a color. IWC greater than 1 ppm was chosen on the basis of agreement between the two IWC measurements on the WB-57F, which also coincided with when total water and water vapor measurements were quite different. Each flight pass through a cloud is uniquely colored. The high IWC found in the early portion of the flight were not colored because they did not belong to the large convective system studied, as determined qualitatively using satellite images

with radar overlay (Figure 3). The first small pass through the convective system was not marked because the CO measurement was in a calibration mode during much of it. Figure 2b shows a typical Argus CO time series with each cloud event marked in the same color as that used in Figure 2a. As IWC increases, so does CO. Lastly, Figure 2c contains altitude plotted against CO with the cloud events still denoted with the same color scheme. The boundary layer CO measurements taken on the Twin Otter are included in Figure 2c to indicate the maximum observed CO values during that day. These measurements include both times when the Twin Otter was near the storm core as well as when under the anvil. This should give an estimate of both an upper and lower limit of what the inflow is into the storm. The two largest cloud events show explicitly that CO is enhanced inside a cloud relative to the free troposphere. The two smaller cloud events also show enhancement of CO in a cloud relative to the free troposphere, but the magnitude is not quite as large. Conversely, as the aircraft leaves the cloud, the CO mixing ratio drops due to dilution with the free tropospheric air. Looking at the data in this manner is acceptable qualitatively, but it does not give a quantitative estimate of the CO transferred to the upper troposphere due to convection.

[17] Another way of analyzing data is examining CO relative to altitude where altitude is binned in 375-m bins (to match the DHARMA model grid spacing). This is demonstrated in Figure 2c using the 29 July 2004 case, where the diamonds represent the altitude-binned in- and out-of-cloud data. There are a few things to note in this plot. First of all, there is overall decrease in CO with increasing altitude, as expected. One also sees a large range in mixing ratios (up to 50 ppb) both in- and out-of-cloud at each altitude. It is also evident that the WB-57F flew level at several altitudes and encountered certain points with high CO relative to the majority of measurements at those altitudes. These CO enhancements were found in the convective anvil cirrus blowoff clouds.

3. Model Description

[18] The Distributed Hydrodynamic-Aerosol-Radiation-Microphysics Application (DHARMA) model [Ackerman *et al.*, 2004; Fridlind *et al.*, 2004; Jensen *et al.*, 2001; Stevens *et al.*, 2002] is a large-eddy dynamics simulation model with embedded size-resolved microphysics. The simulations presented here were designed to provide results that serve to integrate as much microphysical and dynamical information gathered during the experiment as possible. In order to properly represent microphysical processes and their coupling with dynamical processes within computational limits imposed by a typical parallel computing environment (memory and computational burden), these simulations covered a domain just large enough to encompass a relatively small southern Florida cloud system (96 km by 96 km footprint) on each day, with a translating domain to follow the faster-moving systems on 16 and 29 July. Within this domain, resolution was uniform vertically (375 m) and horizontally (1 km), and dynamics were advanced with a 5-s time step. Microphysical processes were represented by tracking the size distribution of aerosols, liquid, and ice, in 16 mass bins within each grid cell. The activation of drops,

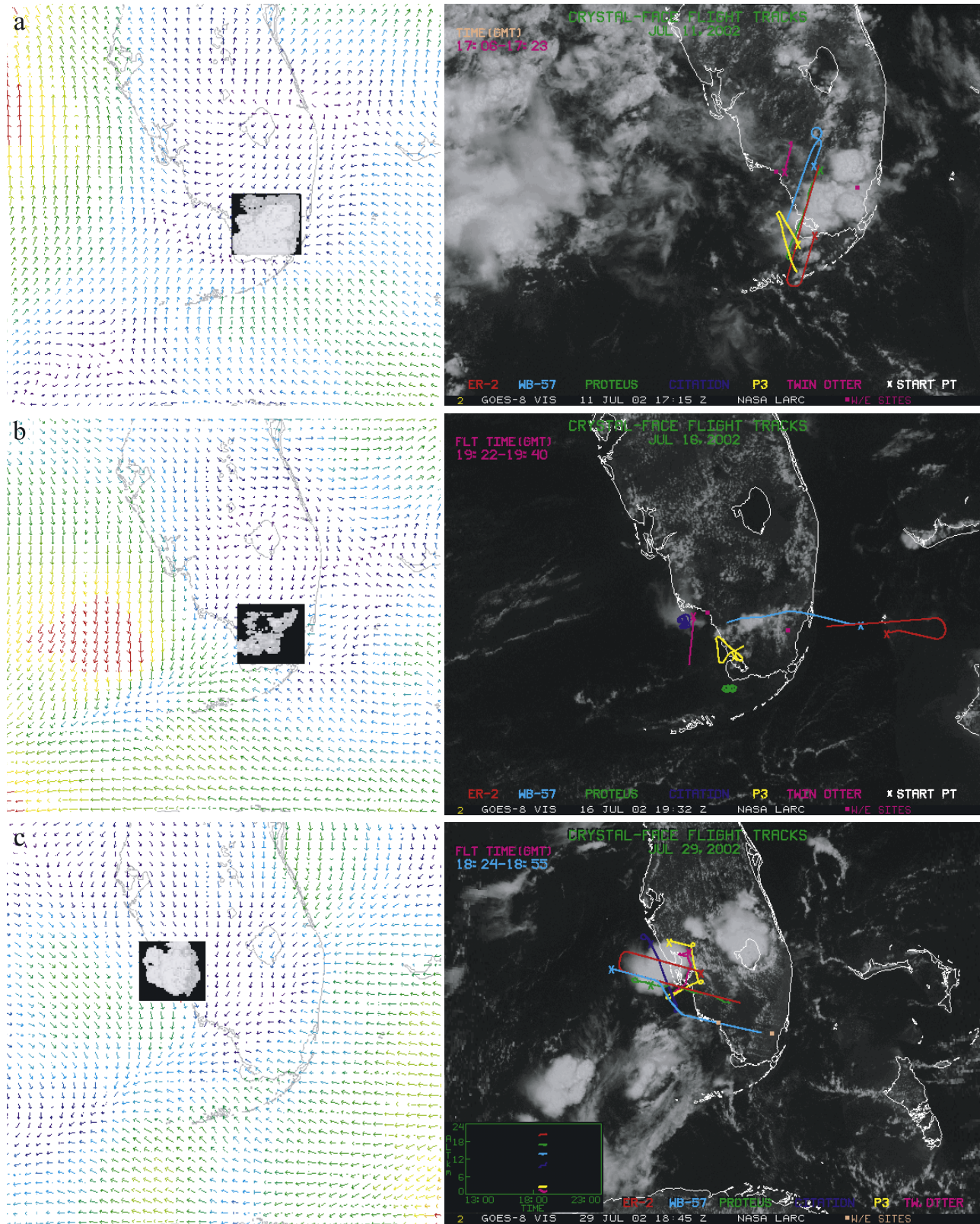


Figure 3. Comparison between simulated convective system and observed system for each flight day: (a) 11 July, (b) 16 July, and (c) 29 July. The left image of each day is the simulated cloud within the DHARMA domain. The right image of each day is a satellite visible image of the convective system with the aircraft flight paths overlaid. These images correspond to the beginning of each day’s relevant flight time.

collision-coalescence, and subsequent multiphase processes were all explicitly advanced with a variable time step (minimum value of 0.2 s). Except for spatial resolution and translation, all details are as described by *Fridlind et al.* [2004]. Aside, we note that the great majority of computational time is spent on microphysical processes (especially collision-coalescence). Solving the fluid dynamics equations and advecting CO and idealized tracers require on the order of 5% of the total computation time, but are crucial to evaluating the accuracy of the dynamical processes, which are in turn important to microphysical processes such as anvil crystal formation, and thus cloud evolution and radiative properties.

4. Evaluation (and Extrapolation) of DHARMA Simulation Results

4.1. Model Setup

[19] As a component of DHARMA model runs to simulate microphysical and dynamical evolution of clouds during CRYSTAL-FACE, CO transport was also calculated with the specific aim of evaluating model representation of entrainment. For each simulation, meteorological initial and time-varying boundary conditions were obtained from forecasts of the Advanced Regional Prediction System (ARPS) mesoscale model [*Xue et al.*, 2003]. Time-varying ARPS model-forecast surface fluxes (15-km horizontal resolution), as well as winds and thermodynamic variables, were used to initialize and nudge the boundaries of the DHARMA model domain (1-km horizontal resolution). Six- to eight-hour simulations were run on each day, with output fields stored at 20-min intervals (Figure 3). Measured CO out-of-cloud vertical profiles were used to initialize the model. Where measurements were not available, DHARMA interpolated between the available measurements as was mostly the case between 6 and 8 km.

4.2. Model Sampling: Overview

[20] Given the DHARMA simulations of these complete diurnal cycles of convection on each day, we then sought a means of using the relatively sparse aircraft observations to evaluate overall model performance. The simple problem with comparing average measured in-cloud CO profiles (over a given flight duration and elevation range) with average simulated in-cloud CO profiles (over a given deep convective event lifetime and elevation range) is that the aircraft actually flew only in thin (or thicker) cirrus at some elevations, or flew only earlier (or later) in the convective cycle on some days. In addition to these day-to-day differences, a simple average of in-cloud model results would always include high-updraft (and high-CO) regions that were entirely avoided by the aircraft. Thus we sought a means of using other variables measured by the aircraft in order to statistically “sample” the simulated clouds in a manner similar to the way in which the aircraft sampled the real clouds, in addition to accounting for flight timing during the convective life cycle. In the remainder of this section, we first theoretically consider possible means of sampling the model domain using other aircraft measurements. We then apply what we consider the best technique to the data on each day. Finally, we calculate a single nonabsolute average difference between the observations

and the sampled model fields in order to quantify overall model performance.

4.3. Temporal Sampling

[21] To begin theoretical consideration of model sampling, we first chose model fields of simulated convection similar to those encountered during the duration of each flight (earlier or later in the diurnal convective cycle) by qualitative evaluation of geostationary satellite images with radar overlay. Because simulated convection timing was not precisely identical to observed timing (differences would be expected simply owing to the use of forecast ARPS fields to drive DHARMA), chosen model times did not precisely match flight times, although durations were the same. Additionally, whereas observations were taken continuously, instantaneous model simulation fields are memory-intensive and were therefore stored only at 20-min simulation time intervals. While most flights lasted 5.5 hours, the relevant flight durations through the convective systems were 1.7 to 3.7 hours. Thus the model results chosen for each day comprised 6 to 12 instantaneous simulation fields.

4.4. Spatial Sampling: Methodology

[22] With the temporal aspect of sampling approximately accounted for, we then chose a simple definition of “in-cloud” for both measurements and simulations (1 ppm of condensate, ice plus water, was considered the cloud boundary, as discussed further in section 2.3), and took a theoretical approach to investigate means of sampling the model spatial domain. In Figure 4, this is demonstrated for the 16 July case. For instance, sampling the model cells with low condensate content intuitively captures the “thickness” of cloud sampled on each flight. Compared with averaging over all in-cloud model cells (Figure 4a, open red circles), averaging over the subset of in-cloud model cells with condensate under 50 ppm (Figure 4a, solid red circles) gives markedly lower mean simulated CO values. Also shown for comparison are the mean observed CO values, which were primarily from the thinner cloud regions with less than 50 ppm condensate.

[23] A particle number concentration filter might also be expected to give a similar effect in capturing thickness. For instance, if we rank the in-cloud (>1 ppm condensate) model cells at each elevation from lowest to highest number concentration, and then consider only those in the lowest 10%, we also obtain a somewhat lower average CO (Figure 4b, solid circles versus open circles). The particle number concentrations were calculated only from model results for theoretical analysis. Aside, here we retain use of condensate to define cloud boundaries, which have elsewhere also been defined in terms of particle number [e.g., *Barth et al.*, 2004].

[24] Finally, we also considered the use of in-cloud (>1 ppm condensate) relative humidity to sample the model results. If we rank the in-cloud model cells at each elevation from lowest to highest relative humidity (calculated only from model results for theoretical analysis), and then consider only those in the lowest 10%, we obtain a drastically lower CO (Figure 3c). In general, these in-cloud cells with lowest relative humidity likely comprise low CO air around the cloud that has received sedimented cloud particles.

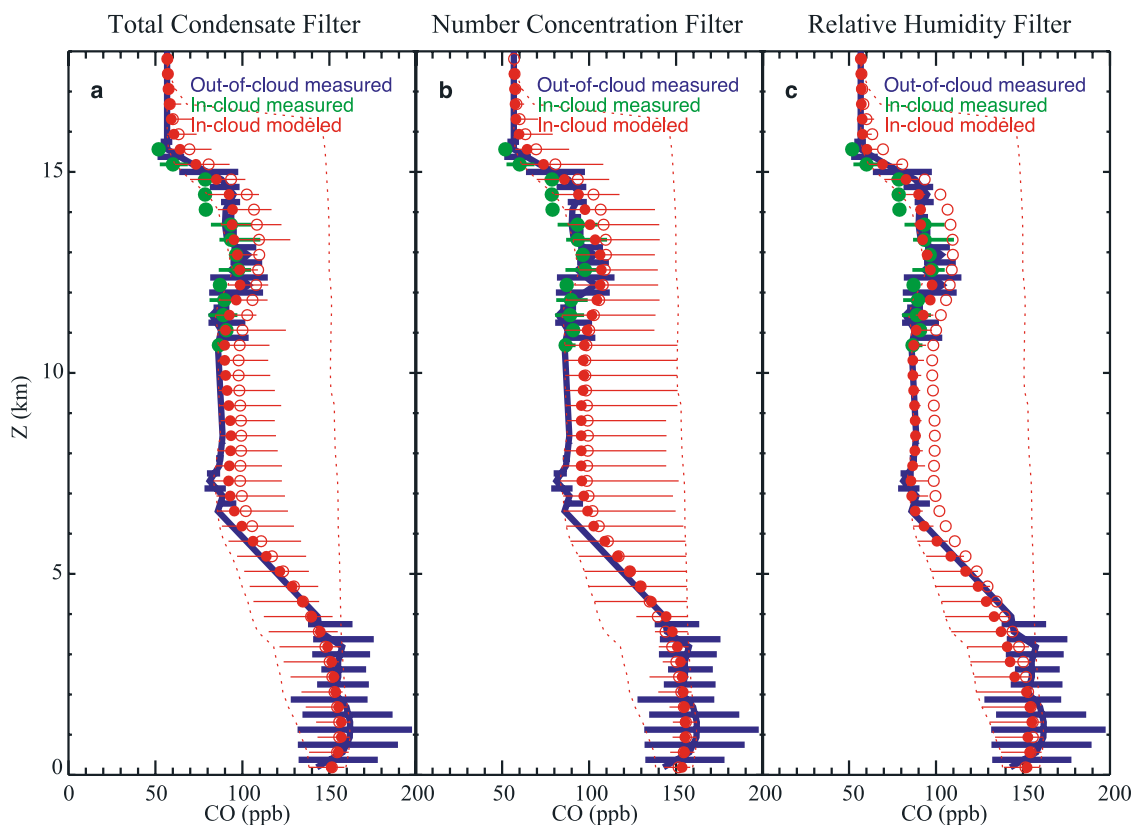


Figure 4. Examples of idealized filters for selection of in-cloud simulations that could be used to quantify the expected bias of aircraft sampling when comparing model results with observations include (a) ice water content (model results < 50 ppm compared with observations), (b) cloud particle number concentration (lowest 10th percentile of model results compared with observations), and (c) relative humidity with respect to ice (lowest 10th percentile of model results compared with observations). The red open circles and dashed lines represent the simulated mean and range of CO in-cloud. The red solid circles and solid lines represent the filtered simulation mean and range of CO in cloud. The green solid circles and line represent the measured mean and range CO in cloud. Last, the blue line represents both the measured and simulated CO out of cloud. Examples of idealized filters are shown for 16 July 2002 with an averaging time of 10 s.

[25] For our actual comparisons, we chose to use total condensate as the simplest means of sampling the model domain, primarily owing to the difficulty of measuring total particle number (distinguishing between large aerosols and small cloud particles, which often dominate total number, may be among the issues) and because in-cloud relative humidity measurements during CRYSTAL-FACE require normalization procedures between in- and out-of-cloud measurements. We thus expected total condensate to be a more reliable measurement in-cloud, and one which we could also use to identify cloud boundaries, for which relative humidity cannot be used, for example.

4.5. Spatial Sampling: Application

[26] Having thus chosen a variable on which to base our model sampling, we advanced from using a simple threshold (such as 50 ppm condensate) to using a histogram weighting function based on flight measurements. Since condensate is entirely ice at the aircraft elevations, we determined IWC for each CO measurement and created from them a histogram of IWC at each elevation. The

histogram thus reflects the range and frequency of cloud thickness encountered by the aircraft at that elevation over the duration of the flight. Because IWC distribution of the observations deviated from the IWC distribution of the model results (Figure 5), we then used the IWC histogram of the observations to sample the model fields by computing a weighted average over the relevant ranges of ice contents, thus averaging over simulated cloud fields of statistically similar “thickness” as observed. Results for all 3 days are shown in Figure 6 and will be discussed in further detail in section 5.

4.6. Performance Evaluation

[27] To evaluate overall model performance in predicting an in-cloud profile similar to observations, we calculated nonabsolute error (E) and the error’s standard deviation (σ_E) for each flight case with the following equations:

$$E = \frac{\sum_z N_z E_z}{\sum_z N_z}$$

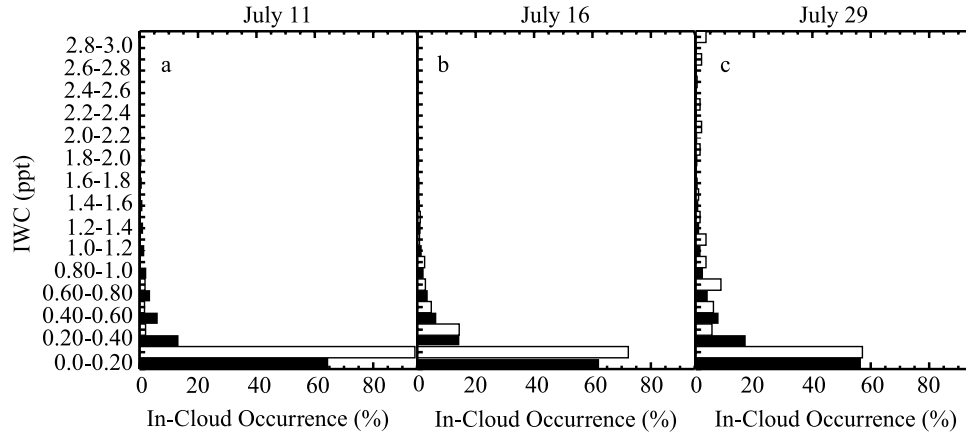


Figure 5. IWC histograms for observations (open bars) and simulations (solid bars) for each flight day: (a) 11 July, (b) 16 July, and (c) 29 July. The histograms demonstrate that the IWC distribution of the observations deviated from the IWC distribution of the model results, as would be expected owing to the sparse sampling by the aircraft. These deviations motivated our overall analysis.

where

$$E_z = \overline{\text{CO}_{\text{simulation},z}} - \overline{\text{CO}_{\text{observation},z}},$$

$$\sigma_E = \sqrt{\frac{\sum_z N_z (E_z - E)^2}{\sum_z N_z}},$$

N_z is the number of observations at each altitude bin, $\overline{\text{CO}_{\text{simulation},z}}$ is the average CO in the model at each altitude bin, and where $\overline{\text{CO}_{\text{observation},z}}$ is the average observed CO at each altitude bin. The observations are binned by altitude in layers that matched model resolution (375 m thickness).

[28] Table 2 summarizes the results of our evaluation. Compared with the case where in-cloud model results were not statistically sampled using IWC (i.e., all simulated in-cloud values were averaged), agreement between model results and observations through use of sampling involving the IWC histograms was approximately 28% improved on 16 July, 39% improved on 29 July and slightly worsened for 11 July. Thus it was important to take the sampling bias of the aircraft into account when using the measurements to evaluate model performance. However, after this bias was accounted for, we found that simulated CO fields still overestimated in-cloud CO on two out of three cases, thus suggesting that DHARMA underestimates entrainment of low-CO free tropospheric air into rising updrafts. Agreement does appear to correlate with the number of measurements available, although the number of days evaluated is not large enough to determine the significance of this trend.

4.7. Sensitivity Tests

[29] We believe that the greatest uncertainty in our simulations is associated with initial and boundary CO fields. These are poorly constrained by measurements, as discussed above, and are therefore also difficult to reasonably bound. We ran three additional simulations (one

for each case) with the minimum likely CO initial profile based on measurements (Table 2), and found that average errors likely are increased or reduced significantly depending on the flight date. Model results continue to appear more frequently biased toward overestimation of CO, with the exception of CO underestimated on 11 July (Table 2).

5. Case Studies

5.1. Study on 11 July 2002

[30] At around 1200 UT (0800 local time), a line of convection developed that was aligned NE-SW over the Everglades with a portion of the storm forming over the west coast of Florida, and with the anvils spreading west of the line of convection. The WB-57F flew into the developing anvil cirrus outflow shortly after their formation. The cirrus was sampled at several levels between 12.5 and 15.5 km (Figure 3a). Unfortunately, Twin Otter boundary layer CO data are not available on this flight day, so a composite of all boundary layer CO data collected in the same region during CRYSTAL-FACE was used. Aircraft observations show enhancement in CO mixing ratios in cloud between 12.5 and 14.0 km, where the aircraft encountered the majority of clouds (Figure 6a). The observed CO mixing ratio enhancement encountered by the WB-57F aircraft in the convective cirrus outflow does not appear as great as on 29 July. This may be for several reasons. Primarily, the observed IWC in the sampled cloud, which can be used as a proxy for cloud “thickness,” reached a maximum of below 1000 ppmv (Figures 1 and 5) indicating that the clouds through which the WB-57F flew were not as thick as on other flights. Secondly, the assumption for modeled boundary layer mixing ratios may have overestimated the actual mixing ratios at higher altitude on that particular day, though there is no direct evidence to support such a supposition. The observed enhancement may actually have been less than on other convective days during CRYSTAL-FACE as suggested by the smaller model-calculated maximum updraft velocity on this day

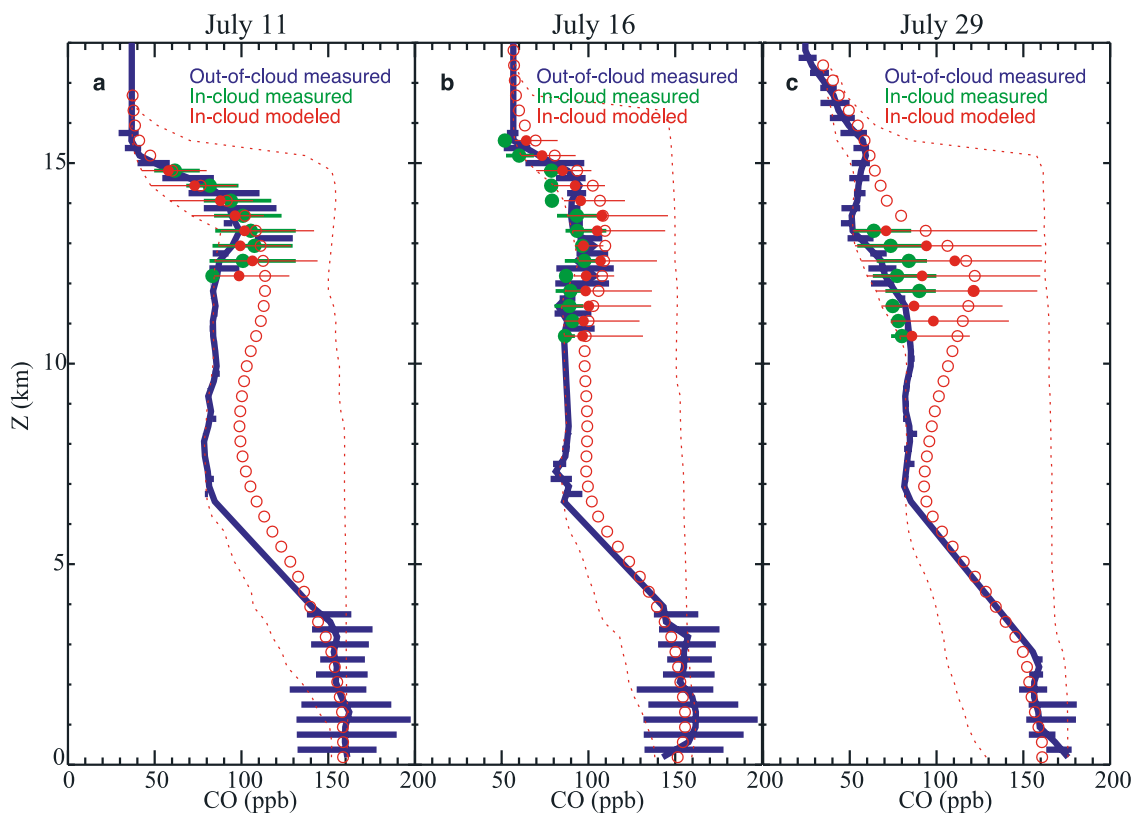


Figure 6. Comparison of observed CO with filtered and unfiltered simulation results. CO measured out-of-cloud by the WB-57F and Twin Otter aircraft was used to initialize the model on each day (blue lines, see text for treatment of missing data): (a) 11 July, (b) 16 July, and (c) 29 July. The mean and full range of subsequent simulated in-cloud values (open red circles and dashed lines) is then compared with the mean and range of measurements by the aircraft on each day (green circles and lines). In addition, the mean and range of in-cloud CO measurements are compared with model results that are sampled with the measured IWC histogram on each day (solid red circles and lines). The effect of aircraft sampling bias is demonstrated in the comparison between the open and solid red circles.

(maximum 30 m/s), thereby venting less boundary layer air early in the storm formation when the WB-57F was sampling the outflow.

[31] The model on this day was able to reproduce the convective storm quite well physically and geographically on the basis of comparison with satellite and radar data (Figure 3a). DHARMA computes in- and out-of-cloud mixing ratios for each altitude range while our sampled data are more sparse (Figure 6a, green circles). In addition,

the model predicts very large ranges of CO in-cloud (Figure 6a, red dashed lines), which are not representative of where the WB-57F was flying. Because of this, the mean in-cloud CO in the model (Figure 6a, open red circles) almost always overpredicts the observed CO with a non-absolute error of 2 ± 5 ppb (Table 2). Using a weighted histogram of observed IWC values during the flight, brings the averaged in-cloud simulated CO values lower than the observed mean CO in the 12–13 km range (Figure 6a, solid

Table 2. Nonabsolute Mean Error and Standard Deviation Between Simulations and Measurements^a

	11 July	16 July	29 July	Overall
Duration, h:min	3:20	3:40	1:40	
Observations, number	538	392	196	
Error using all in-cloud model results				
Mean measured CO case, ppb	2 ± 5	14 ± 3	33 ± 4	12 ± 4
Error using IWC to weight model results				
Mean measured CO case, ppb	-4 ± 4	10 ± 2	20 ± 11	5 ± 5
Minimum measured CO case, ppb	-14 ± 6	1 ± 3	13 ± 10	-4 ± 6
130-ppb boundary layer CO case, ppb			5 ± 6	

^aError calculation and cases are described in the text.

red circles). However, the nonabsolute average error using the IWC filter was -4 ± 4 ppb, which was not much different than the unfiltered case (Table 2).

5.2. Study on 16 July 2002

[32] A relatively isolated convection system and its persistent anvil were sampled extensively on 16 July by the WB-57F. Convection formed in south central Florida (mostly over the Everglades) at around 1930 UT and developed a fast-moving anvil that traversed to the west. While this was the most extensively sampled convective outflow, the boundary layer air was relatively clean due to the location of the storm formation and not downwind of any urban or industrialized areas (Figure 3b). As on 11 July, Twin Otter data were not available and a composite boundary layer CO mixing ratio sampled in the same region was therefore used (the same CO boundary layer profile as used for 11 July). In addition, the Climate Monitoring and Diagnostics Laboratory (CMDL) ground site (Key Biscayne, Florida) sampled the boundary layer air slightly upwind (inflow) of the storm formation and found that CO at the ground was quite low (around 84 ppb) on this day (P. Novelli, personal communication, 2002). During most of the WB-57F's high-altitude flight, the convection cirrus outflow was sampled at around 13.5 km. The highest enhancements in CO were observed during the flight in the 12.5–13.5 km region. The observed enhancements, however, were not as large as those found on 11 July (Figure 6b), likely due to the formation of convection in relatively clean air (which was not captured by the CO boundary profile used to initialize the model). The fact that the enhancements were actually observed can be attributed to the “thickness” in the cloud layer we sampled (IWC maximum between 2000 and 3000 ppm, Figure 1). A similar study was performed on CO₂ for this convective storm [Xueref *et al.*, 2004] in which CO₂ was found to decrease by about 0.5 ppm in the 12.5–13.5 km range. That study, however, was not constrained by boundary layer observations. The maximum updraft velocity in the simulations reached near 40 m/s, which was higher than that during 11 July. Temporally, this convective system was studied from its formation until it nearly dissipated. It was the best sampled convective system during CRYSTAL-FACE, but CO enhancement from convective transport was minimal. The earlier portions of the WB-57F flight demonstrated greater CO enhancement than later portions (not shown), but this information is lost here by binning the full flight by altitude.

[33] The DHARMA model results for this convective system, both in- and out-of-cloud can again be found in Figure 5b. The model was able to reproduce the convective storm quite well both physically and spatially as determined by satellite and radar data (Figure 3b). The average in-cloud CO mixing ratios were once more overpredicted and had an error of 14 ± 3 ppb (Table 2). The maximum convectively transported CO, however, was predicted at the same altitude range as the observations. Despite extensive sampling, the increased error may be due to the overestimated CO boundary layer profile, as low CO observations are not represented by the model. Using the IWC measurements to statistically sample the model results, the over prediction is decreased and the error is reduced by $\sim 30\%$ (Figure 6b and

Table 2). Because most of the flight was spent between 12 and 13.5 km, there were not many observations at higher and lower altitudes. The in-cloud observations outside of that altitude range may not have been sampled enough to be statistically significant. It is, thereby, not surprising that the best model observation agreement is found in 12–13.5 km altitude range.

5.3. Study on 29 July 2002

[34] There was a significant thunderstorm that formed north of Naples, Florida between 1700 and 1730 UT on 29 July and moved northward along the west coast of Florida. The storm was largely offshore even in its initial stages and the system produced an extensive cloud deck moving NW off the Florida coast throughout the rest of the afternoon. This storm eventually merged with a convective system, which formed over Lake Okeechobee. The Twin Otter aircraft directly probed below the cloud bases in the thunderstorm activities along the west coast of Florida, so we may have direct measurements of both early and late stage boundary layer air input into the convective turret (Figure 3c). At all altitudes where the WB-57F flew into anvil outflow, a large enhancement of CO (10–15 ppb) relative to the free troposphere was observed (Figure 6c). In fact, this flight showed the largest observed enhancement of CO mixing ratios of any flight during CRYSTAL-FACE. This is not surprising as a majority of this storm formed over a relatively well populated area and the anvil blow off sampled was quite thick (IWC maximum of 3800 ppm, Figure 1) relative to all other flights. In addition, the simulated updraft velocity was almost double that of the other two cases, with a maximum velocity of near 60 m/s. The observed CO enhancement was located between 11.5 and 13.3 km. The WB-57F did not sample the convective system higher than 13.3 km.

[35] The unfiltered DHARMA simulation of this convective system, both in- and out-of-cloud modeled means and their respective ranges are shown in Figure 6c. The model on this day was able to reproduce the convective storm quite well physically and geographically, as determined by satellite and radar (Figure 3c). In the DHARMA simulation, the in-cloud CO mixing ratios were largely overpredicted at all altitudes. The model does, however, again predict the maximum convection-transported CO in the same 11.5–13.5 km region with the peak at 12 km. While this was the strongest observed case of CO enhancement due to convective transport, it was also the least characterized system. The model's overprediction of CO may have related to the peak updraft conditions on 29 July. Using the previously described IWC filter, most of the mean CO from the model approached the observed values but still overpredicted the observations (Figure 6c). The error decreased by 39% using the IWC filter to sample the model (Table 2). That the error was not reduced more may be due to sparse sampling during flight that did not acquire enough IWC values for a statistically significant histogram. Interestingly, using just the tenth percentile of model relative humidity actually works quite well in this case (not shown). We, however, do not have actual relative humidity observations with which to constrain the model and can only do a sensitivity test, as

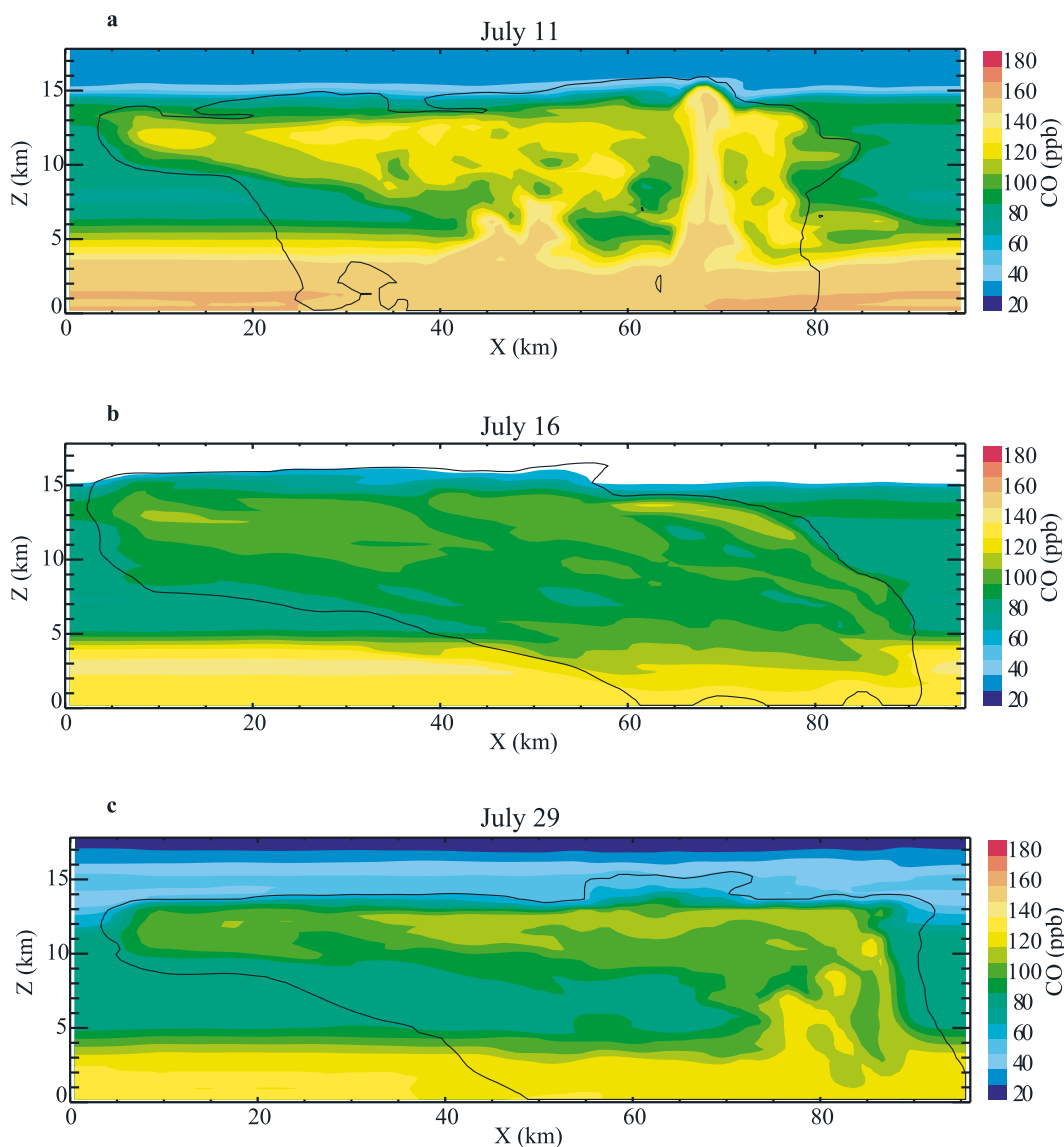


Figure 7. Instantaneous cross section of the three-dimensional model simulations, at a time corresponding to the middle of each flight, at the model location of peak total CO in the convective cores for each flight day: (a) 11 July, (b) 16 July, and (c) 29 July. The simulation used corresponds to that which provided lowest error (base case on 11 July and minimum CO sensitivity tests on 16 and 29 July, see Table 2).

described in section 4. Since this storm formed partially over water, we ran an additional simulation (sensitivity test) with the boundary layer air consisting of 130 ppb CO (minimum CO), which is a more realistic value for marine layer CO. The simulation results, while approaching the observations, still overpredict the CO, although, the extent was much smaller (Table 2).

6. Summary and Conclusions

[36] Large convective storms found in the midlatitudes, subtropics, and tropics can efficiently redistribute boundary layer air to the upper troposphere. The redistribution of trace gases, especially H_2O to the upper troposphere, can change its chemical and radiative properties. It is therefore important to understand how much boundary layer air reaches the

free and upper troposphere. CO can be used as a tracer for boundary air and its degree of dilution because its chemical lifetime is long relative to the transport times of air through convective systems.

[37] During CRYSTAL-FACE, convective systems were only sampled in the cirrus outflows and not in the cores. Consequently, observed CO enhancements were not quite as large as seen in previous studies [i.e., Dickerson *et al.*, 1987]. Furthermore, observed enhancements were diminished due to the relatively clean boundary layer inflow to the convective systems. While we do not have measurements of CO in the cores of these convective systems, the maximum CO levels can be estimated from the model results. Assuming that the initial CO vertical profile in noncloudy air input into DHARMA is correct, maximum CO in the core of the storms on 11, 16, and 29 July can be

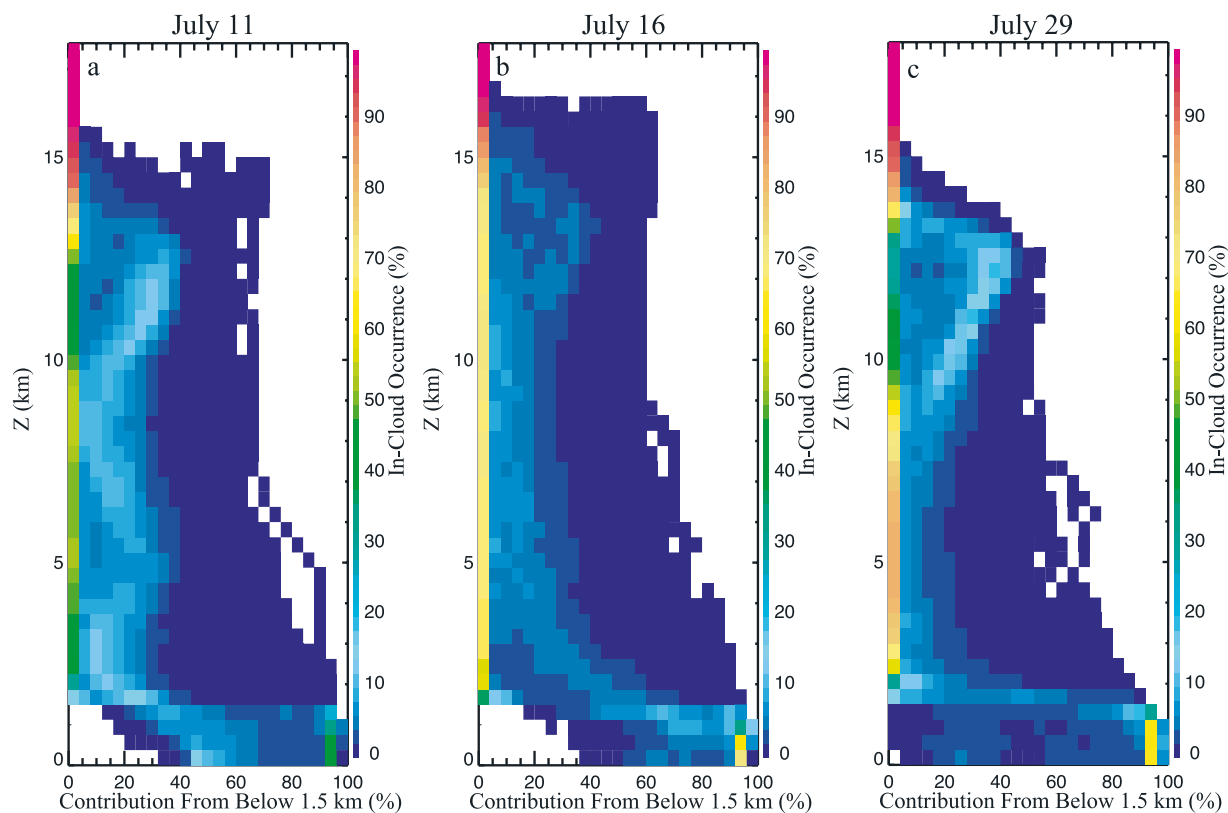


Figure 8. (a–c) Histogram of boundary layer contribution to in-cloud air, estimated using an idealized tracer initialized to 1.0 below 1.5 km and zero elsewhere (see section 6). These plots correspond to the same time and simulations used in Figure 7.

approximated as 160, 130, and 120 ppb, respectively (Figure 7), where the plotted model cross sections correspond to the middle of each flight temporally, at the horizontal model location where peak lofted CO was found. In addition, the cross sections correspond to the simulations that provided the lowest error (Table 2). This includes using the lowest CO out-of-cloud vertical profiles for 16 and 29 July, and the baseline simulation for 11 July. The maximum CO values were found between 12 and 13.5 km, and were 18, 15, and 17% larger than peak CO observations at those same altitudes. The peak simulated CO in the storm outflow on each flight day was approximately 120, 110, and 110 ppb respectively. 11 July was underpredicted in the outflow by 10%, which explains why the error increased when using IWC during the analysis (Table 2). The CO for 16 July, being the best sampled convective system, exhibited less than 2% difference between the maximum observed CO and the peak modeled CO in the outflow. The strongest convective case, 29 July, was overpredicted by 10% in the outflow.

[38] Because CO tracer observations were limited spatially and temporally relative to the simulated convective systems, idealized tracers were used to estimate how much boundary layer air contributed to the in-cloud air at each altitude range. These idealized tracers were initialized to 1.0 below 1.5 km and zero elsewhere. The boundary layer air contribution was evaluated at the same simulated storm time as in Figure 7. These results are shown in Figures 8a–8c. They are displayed as histograms that show what percentage of

the air at each altitude range contained a certain percentage of boundary layer air. For example, on 29 July, at 12 km, anvil air parcels contained up to 60% boundary layer air. Maximum contributions of boundary layer air at anvil levels were usually ~ 60 –70%, but these amounts occurred in only a very small percentage of grid cells. In general, the free tropospheric cloudy anvil air contained 20–40% boundary layer air, with the majority of the air entrained from the free troposphere. This result is similar to other studies [Dickerson *et al.*, 1987; Mari *et al.*, 2003; Scala *et al.*, 1990; Wang and Chang, 1993; Wang *et al.*, 1995] where sampling of the convective systems was closer to the core of the storm. Estimating both the maximum CO transported in the core of a storm and the percentage of boundary layer air reaching each altitude is important, especially under the sparse and nonideal sampling conditions during CRYSTAL-FACE.

[39] The work presented in this paper helps understand how much boundary layer air has reached the upper troposphere using less-than-ideal measurements. In this paper, we studied three convective systems that occurred during the CRYSTAL-FACE campaign. We modeled the convective systems with a cloud-resolving model using observational filters to sample the simulation results in a manner consistent with observations. A nonabsolute error and its standard deviation were calculated for each simulation on each day and an overall error was calculated for each case. We found that IWC measurements can be used as a powerful filter under nonideal sampling conditions.

[40] In future experiments, better sampling in the inflow region of the convective system could better constrain boundary layer conditions. In addition, sampling at or near the core of the storm as well as in the outflow would help to indicate how much boundary layer air reached the upper troposphere and how quickly the CO is diluted from the maximum in the core. Furthermore, better sampling over a large altitude range is necessary in the free troposphere to establish boundary conditions on free tropospheric inflow to convective storms. In addition, such studies could be augmented with more tracers, such as O₃, assuming availability of boundary layer measurements. The resulting knowledge of the distribution of a long-lived tracer will be highly beneficial to the interpretation of detailed measurements to better understand transport processes like convective redistribution of gases. However, in the absence of better sampling conditions, we have demonstrated a powerful technique to sample model results in order to better analyze and extrapolate observations under nonideal sampling conditions.

[41] **Acknowledgments.** This work was supported by the NASA Radiation Science program. We thank the CRYSTAL-FACE Science and Support team for helpful discussions during and after the field mission. This research was performed while the first author held a National Research Council Research Associateship Award at NASA Ames Research Center.

References

- Ackerman, A. S., M. P. Kirkpatrick, D. E. Stevens, and O. B. Toon (2004), The impact of humidity above stratiform clouds on indirect aerosol climate forcing, *Nature*, *432*, 1014–1017.
- Barth, M. C., A. L. Stuart, and W. C. Skamarock (2001), Numerical simulations of the July 10 Stratospheric-Tropospheric Experiment: Radiation, aerosols and ozone/deep convection storm: Redistribution of soluble tracers, *J. Geophys. Res.*, *106*, 12,381–12,400.
- Barth, M. C., S. Kim, C. Wang, A. Fridlind, J. Pinty, C. Mari, S. Cautenet, V. Spiridonov, K. Pickering, and L. Ott (2004), Summary of the Chemistry Transport in Deep Convection Cloud Modeling Workshop intercomparison, *Eos Trans. AGU*, *85*(47), Fall Meet. Suppl., Abstract A21C-0754.
- Bernardet, L. R., L. D. Grasso, J. E. Nachamkin, C. A. Finley, and W. R. Cotton (2000), Simulating convective events using a high-resolution mesoscale model, *J. Geophys. Res.*, *105*(D11), 14,963–14,982.
- Chatfield, R. B., and P. J. Crutzen (1984), Sulfur dioxide in the remote oceanic air: Cloud transport of reactive precursors, *J. Geophys. Res.*, *89*(D5), 7111–7132.
- Danielson, E. F. (1993), In situ evidence of rapid, vertical, irreversible transport of lower tropospheric air into the lower tropical stratosphere by convective cloud turrets and by larger-scale upwelling in tropical cyclones, *J. Geophys. Res.*, *98*(D5), 8665–8681.
- DeCaria, A. J., K. E. Pickering, G. L. Stenchikov, J. R. Scala, J. L. Stith, J. E. Dye, B. A. Ridley, and P. Laroche (2000), A cloud-scale model study of lightning-generated NO_x in an individual thunderstorm during STERAO-A, *J. Geophys. Res.*, *105*(D9), 11,601–11,616.
- DeCaria, A. J., K. E. Pickering, G. L. Stenchikov, and L. E. Ott (2005), Lightning-generated NO_x and its impact on tropospheric ozone production: A three-dimensional modeling study of a Stratosphere-Troposphere Experiment: Radiation, Aerosols and Ozone (STERAO-A) thunderstorm, *J. Geophys. Res.*, *110*, D14303, doi:10.1029/2004JD005556.
- Dickerson, R. R., et al. (1987), Thunderstorms: An important mechanism in the transport of air pollutants, *Science*, *235*(4787), 460–465.
- Dye, J. E., et al. (2000), An overview of the Stratospheric-Tropospheric Experiment: Radiation, aerosols and ozone (STERAO)-Deep Convection experiment with results for the July 10, 1996 storm, *J. Geophys. Res.*, *105*(D8), 10,023–10,045.
- Fehr, T., H. Höller, and H. Huntrieser (2004), Model study on production and transport of lightning-produced NO_x in a EULINOX supercell storm, *J. Geophys. Res.*, *109*, D09102, doi:10.1029/2003JD003935.
- Fenn, M. A., et al. (1999), Ozone and aerosol distributions and air mass characteristics over the South Pacific during the burning season, *J. Geophys. Res.*, *104*(D13), 16,197–16,212.
- Fischer, H., et al. (2003), Deep convective injection of boundary layer air into the lowermost stratosphere at midlatitudes, *Atmos. Chem. Phys.*, *3*, 739–745.
- Folkens, I., R. Chatfield, D. Baumgardner, and M. Proffitt (1997), Biomass burning and deep convection in southeastern Asia: Results from ASHOE/MAESA, *J. Geophys. Res.*, *102*(D11), 13,291–13,299.
- Fridlind, A. M., et al. (2004), Evidence for the predominance of mid-tropospheric aerosols as subtropical anvil cloud nuclei, *Science*, *304*, 718–722.
- Garstang, M., et al. (1988), Trace gas exchange and convective transports over the Amazonian rain forest, *J. Geophys. Res.*, *93*(D2), 1528–1550.
- Gerbig, C., S. Schmitgen, D. Kley, A. Volz-Thomas, K. Dewey, and D. Haaks (1999), An improved fast-response vacuum-UV resonance fluorescence CO instrument, *J. Geophys. Res.*, *104*(D1), 1699–1704.
- Gimson, N. R. (1997), Pollution transport by convective clouds in a mesoscale model, *Q. J. R. Meteorol. Soc.*, *123*(542), 1805–1828.
- Hallar, A. G., L. M. Avallone, R. L. Herman, B. E. Anderson, and A. J. Heymsfield (2004), Measurements of ice water content in tropopause region Arctic cirrus during the SAGE III Ozone Loss and Validation Experiment (SOLVE), *J. Geophys. Res.*, *109*, D17203, doi:10.1029/2003JD004348.
- Hauf, T., P. Schulte, R. Alheit, and H. Schlager (1995), Rapid vertical trace gas transport by an isolated midlatitude thunderstorm, *J. Geophys. Res.*, *100*(D11), 22,957–22,970.
- Herman, R. L., et al. (2002), Hydration, dehydration, and the total hydrogen budget of the 1999/2000 winter Arctic stratosphere, *J. Geophys. Res.*, *108*(D5), 8320, doi:10.1029/2001JD001257.
- Jacob, D. J., J. H. Crawford, M. M. Kleb, V. S. Connors, R. J. Bendura, J. L. Raper, G. W. Sachse, J. C. Gille, L. Emmons, and C. L. Heald (2003), Transport and Chemical Evolution over the Pacific (TRACE-P) aircraft mission: Design, execution, and first results, *J. Geophys. Res.*, *108*(D20), 8827, doi:10.1029/2002JD003075.
- Jensen, E. J., L. Pfister, A. S. Ackerman, and O. B. Toon (2001), A conceptual model of the dehydration of air due to freeze-drying by optically thin, laminar cirrus rising slowly across the tropical tropopause, *J. Geophys. Res.*, *106*(D15), 17,237–17,252.
- Jensen, E., D. Starr, and O. B. Toon (2004), Mission investigates tropical cirrus clouds, *Eos Trans. AGU*, *85*, 45–50.
- Kiley, C. M., et al. (2003), An intercomparison and evaluation of aircraft-derived and simulated CO from seven chemical transport models during the TRACE-P experiment, *J. Geophys. Res.*, *108*(D21), 8819, doi:10.1029/2002JD003089.
- Lin, X., B. A. Ridley, J. Walega, G. F. Hübler, S. A. McKeen, E.-Y. Hsie, M. Trainer, F. C. Fehsenfeld, and S. C. Liu (1994), Parameterization of subgrid scale convective cloud transport in a mesoscale regional chemistry model, *J. Geophys. Res.*, *99*(D12), 25,615–25,630.
- Liu, H., D. J. Jacob, I. Bey, R. M. Yantosca, B. N. Duncan, and G. W. Sachse (2003), Transport pathways for Asian pollution outflow over the Pacific: Interannual and seasonal variation, *J. Geophys. Res.*, *108*(D20), 8786, doi:10.1029/2002JD003102.
- Loewenstein, M., H. Jost, J. Grose, J. Eilers, D. Lynch, S. Jensen, and J. Marmie (2002), Argus: A new instrument for the measurement of the stratospheric dynamical tracers, N₂O and CH₄, *Spectrochim. Acta A*, *58*(11), 2329–2345.
- Luke, W. T., R. R. Dickerson, W. F. Ryan, K. E. Pickering, and L. Nunnemacker (1992), Tropospheric chemistry over the great plains of the United States: 2. Trace gas profiles and distributions, *J. Geophys. Res.*, *97*(D18), 20,647–20,670.
- Mari, C., D. J. Jacob, and P. Bechtel (2000), Transport and scavenging of soluble gases in a deep convective cloud, *J. Geophys. Res.*, *105*(D17), 22,255–22,268.
- Mari, C., et al. (2003), On the relative role of convection, chemistry, and transport over the South Pacific Convergence Zone during PEM-Tropics B: A case study, *J. Geophys. Res.*, *107*(D2), 8232, doi:10.1029/2001JD001466.
- Park, R. J., K. E. Pickering, D. J. Allen, G. L. Stenchikov, and M. S. Fox-Rabinovitz (2004), Global simulation of tropospheric ozone using the University of Maryland Chemical Transport Model (UMD-CTM): 1. Model description and evaluation, *J. Geophys. Res.*, *109*, D09303, doi:10.1029/2003JD004269.
- Pickering, K. E., R. R. Dickerson, G. J. Huffman, J. F. Boatman, and A. Schanot (1988), Trace gas transport in the vicinity of frontal convective clouds, *J. Geophys. Res.*, *93*(D1), 759–773.
- Pickering, K. E., R. R. Dickerson, W. T. Luke, and L. J. Nunnemacker (1989), Clear-sky vertical profiles of trace gases as influenced by upstream convective activity, *J. Geophys. Res.*, *94*(D12), 14,879–14,892.
- Pickering, K. E., A. M. Thompson, R. R. Dickerson, W. T. Luke, and D. P. McNamara (1990), Model calculations of tropospheric ozone production potential following observed convective events, *J. Geophys. Res.*, *95*(D9), 14,049–14,062.

- Pickering, K. E., A. M. Thompson, J. R. Scala, W.-K. Tao, J. Simpson, and M. Garstang (1991), Photochemical ozone production in tropical squall line convection during NASA Global Tropospheric Experiment/Amazon Boundary Layer Experiment 2A, *J. Geophys. Res.*, *96*(D2), 3099–3114.
- Pickering, K. E., A. M. Thompson, J. R. Scala, R. R. Dickerson, and J. Simpson (1992), Free tropospheric ozone production following entrainment of urban plumes into deep convection, *J. Geophys. Res.*, *97*(D16), 17,985–18,000.
- Pickering, K. E., A. M. Thompson, W.-K. Tao, and T. L. Kucsera (1993), Upper tropospheric ozone production following mesoscale convection during STEP/EMEX, *J. Geophys. Res.*, *98*(D5), 8737–8749.
- Pickering, K. E., A. M. Thompson, W.-K. Tao, R. B. Rood, D. P. McNamara, and A. M. Molod (1995), Vertical transport by convective clouds: Comparison of three modeling approaches, *Geophys. Res. Lett.*, *22*(9), 1089–1092.
- Pickering, K. E., et al. (1996), Convective transport of biomass burning emissions over Brazil during TRACE A, *J. Geophys. Res.*, *101*(D19), 23,993–24,012.
- Pickering, K. E., Y. Wang, W.-K. Tao, C. Price, and J.-F. Müller (1998), Vertical distribution of lightning NO_x for use in regional and global chemical transport models, *J. Geophys. Res.*, *103*(D23), 31,203–31,216.
- Pickering, K. E., et al. (2001), Trace gas transport and scavenging in PEM-Tropics B South Pacific Convergence Zone convection, *J. Geophys. Res.*, *106*(D23), 32,591–32,607.
- Poulida, O., R. R. Dickerson, and A. Heymsfield (1996), Stratosphere-troposphere exchange in a midlatitude mesoscale convective complex: 1. Observations, *J. Geophys. Res.*, *101*(D3), 6823–6836.
- Prather, M. J., and D. J. Jacobs (1997), A persistent imbalance in HO_x and NO_x photochemistry of the upper troposphere driven by deep tropical convection, *Geophys. Res. Lett.*, *24*, 3189–3192.
- Randriambelo, T., J.-L. Baray, and S. Baldy (2000), Effect of biomass burning, convective venting and transport on tropospheric ozone over the Indian Ocean: Reunion Island field observations, *J. Geophys. Res.*, *105*(D9), 11,813–11,832.
- Scala, J. R., W.-K. Tao, A. M. Thompson, J. Simpson, M. Garstang, K. E. Pickering, E. V. Browell, G. W. Sachse, G. Gregory, and A. Torres (1990), Cloud draft structure and trace gas transport, *J. Geophys. Res.*, *95*(D10), 17,015–17,030.
- Skamarock, W. C., J. G. Powers, M. Barth, J. E. Dye, T. Matejka, D. Bartels, K. Baumann, J. Stith, D. D. Parrish, and G. Hubler (2000), Numerical simulations of the July 10 Stratospheric-Tropospheric Experiment: Radiation, Aerosols, and Ozone/Deep Convection Experiment convective system: Kinematics and transport, *J. Geophys. Res.*, *105*(D15), 19,973–19,990.
- Smyth, S., et al. (1996), Comparison of free tropospheric western Pacific air mass classification schemes for the PEM-West A experiment, *J. Geophys. Res.*, *101*(D1), 1743–1762.
- Stenchikov, G. J., B. Doddridge, S. Kondragunta, O. Poulida, J. Scala, and W.-K. Tao (1996), Stratosphere-troposphere exchange in a midlatitude mesoscale convective complex: 2. Numerical simulations, *J. Geophys. Res.*, *101*(D3), 6837–6852.
- Stevens, D. E., A. S. Ackerman, and C. S. Bretherton (2002), Effect of domain size and numerical resolution on the simulation of shallow cumulus convection, *J. Atmos. Sci.*, *59*, 3285–3301.
- Thompson, A. M., K. E. Pickering, R. R. Dickerson, W. G. Ellis Jr., D. J. Jacob, J. R. Scala, W.-K. Tao, D. P. McNamara, and J. Simpson (1994), Convective transport over the central United States and its role in regional CO and ozone budgets, *J. Geophys. Res.*, *99*(D9), 18,703–18,711.
- Thompson, A. M., K. E. Pickering, D. P. McNamara, M. R. Schoerberl, R. D. Hudson, J. H. Kim, E. V. Browell, W. J. H. W. Kirchhoff, and D. Nganga (1996), Where did tropospheric ozone over southern Africa and the tropical Atlantic come from in October 1992? Insights from TOMS, GTE, TRACE A, and SAFARI 1992, *J. Geophys. Res.*, *101*(D19), 24,251–24,278.
- Thompson, A. M., W.-K. Tao, K. E. Pickering, J. R. Scala, and J. Simpson (1997), Tropical deep convection and ozone formation, *Bull. Am. Meteorol. Soc.*, *78*(6), 1043–1054.
- Wang, C., and J. S. Chang (1993), A three-dimensional numerical model of cloud dynamics, microphysics, and chemistry: 3. Redistribution of pollutants, *J. Geophys. Res.*, *98*(D9), 16,787–16,798.
- Wang, C., and P. Crutzen (1995), Impact of a simulated severe local storm on the redistribution of sulfur dioxide, *J. Geophys. Res.*, *100*(D6), 11,357–11,368.
- Wang, C., and R. G. Prinn (1998), Impact of the horizontal wind profile on the convective transport of chemical species, *J. Geophys. Res.*, *103*(D17), 22,063–22,072.
- Wang, C., P. J. Crutzen, V. Ramanathan, and S. F. Williams (1995), The role of a deep convective storm over the tropical Pacific Ocean in the redistribution of atmospheric chemical species, *J. Geophys. Res.*, *100*(D6), 11,509–11,516.
- Wang, Y., S. C. Liu, H. Yu, S. T. Sandholm, T.-Y. Chen, and D. R. Blake (2000), Influence of convection and biomass burning outflow on tropospheric chemistry over the tropical Pacific, *J. Geophys. Res.*, *105*(D7), 9321–9334.
- Weinstock, E. M., E. J. Hints, A. E. Dessler, J. F. Oliver, N. L. Hazen, J. N. Demusz, N. T. Allen, L. B. Lapsen, and J. G. Anderson (1994), New fast-response photofragment fluorescence hygrometer for use on the NASA ER-2 and the Perseus remotely piloted aircraft, *Rev. Sci. Instrum.*, *65*, 3544–3554.
- Xue, M., D.-H. Wang, J.-D. Gao, K. Brewster, and K. K. Droegemeier (2003), The Advanced Regional Prediction System (ARPS), storm-scale numerical weather prediction and data assimilation, *Meteorol. Atmos. Phys.*, *82*, 139–170.
- Xueref, I., et al. (2004), Combining a receptor-oriented framework for tracer distributions with a cloud-resolving model to study transport in deep convective clouds: Application to the NASA CRYSTAL-FACE campaign, *Geophys. Res. Lett.*, *31*, L14106, doi:10.1029/2004GL019811.
- A. S. Ackerman, A. M. Fridlind, A. G. Hallar, and M. Loewenstein, NASA Ames Research Center, Moffett Field, CA 94035, USA.
- L. M. Avallone and S. M. Davis, Program in Atmospheric and Oceanic Sciences, University of Colorado, Boulder, CO 80309-0590, USA.
- T. L. Campos, National Center for Atmospheric Research, Boulder, CO 80303, USA.
- R. L. Herman, Jet Propulsion Lab, Pasadena, CA 91109, USA.
- H.-J. Jost and J. P. Lopez, Bay Area Environmental Research Institute, Sonoma, CA 95476, USA. (jlopez@mail.arc.nasa.gov)
- J. V. Pittman, D. S. Sayres, J. B. Smith, and E. M. Weinstock, Department of Earth and Planetary Sciences, Harvard University, Cambridge, MA 02138, USA.